Ordered Polyelectrolyte "Multilayers". 1. Mechanisms of Growth and Structure Formation: A Comparison with Classical Fuzzy "Multilayers"

X. Arys,[†] A. Laschewsky,[‡] and A. M. Jonas*[,†]

Unité de physique et de chimie des hauts polymères, Université catholique de Louvain, Place Croix du Sud, 1, B-1348 Louvain-la-Neuve, Belgium (European Union), and Unité de chimie des matériaux, Université catholique de Louvain, Place Louis Pasteur, 1, B-1348 Louvain-la-Neuve, Belgium (European Union)

Received January 18, 2001; Revised Manuscript Received February 5, 2001

ABSTRACT: The growth and structuring of polyelectrolyte self-assemblies (so-called "multilayers") made from a lyotropic ionene and a strong polyelectrolyte are examined in depth using X-ray reflectometry among other techniques. We show that highly ordered polyelectrolyte films may be obtained, consisting of a regular lamellar nanostructure extending over considerable distances in the films, with preferential orientation of chain fragments occurring in the films. This is in marked contrast with classical, "fuzzy" multilayers, for which no internal structure was reported so far. From our set of results, including a comparison of the structures of "multilayers" and bulk complexes, we propose that three mechanisms govern film growth and structuring: adsorption of the polyelectrolyte (governed by electrostatic balance), diffusion of the polyelectrolyte into the previously adsorbed film (which is the blurring step), and surface-constrained complexation between the polyanion and the polycation resulting from the mixing due to diffusion. Depending on whether the polyelectrolytes are capable of forming structured complexes or not, the self-assembled film will present different levels of internal organization. These findings have important implications for the general understanding of electrostatic self-assembly and for possible applications therefrom.

Introduction

In recent years, significant progress has been achieved in the preparation and characterization of organic and hybrid organic−inorganic ultrathin multilayers (MLs). The growing interest in these systems, stemming from both fundamental and applied interests, is partly due to unusual physical properties of nanostructured materials and to potential applications resulting from these properties, in particular in the field of integrated molecular optics, electronics, and biosensors.[1] Presently, a number of methods exist for the preparation of organic multilayers, among which the Langmuir−Blodgett (LB)[2,3] and chemical self-assembly[2,4] methods have probably generated the largest number of publications.

In this context, electrostatic self-assembly (ESA) has been developed recently[5] as a new way for producing ultrathin organic or hybrid organic−inorganic supramolecular assemblies with angstrom precision, without requiring expensive equipment. Recent reviews[6−15] highlight the potential and limitations of ESA. The technique, based on the alternate adsorption of charge-bearing molecules or particles, is particularly remarkable with respect to its very large applicability: for example, reports were published early on films prepared from electroactive polymers,[16] proteins,[17] DNA,[18] dyes,[19] inorganic platelets,[20] latex particles,[21] dendrimers,[22] fullerenes,[23] and even viruses.[24] Furthermore, there is practically no limitation on shape and nature of substrates, as testified for example by numerous reports on the fabrication of polyelectrolyte micro- and nanocapsules via the growth of such multilayers on colloids.[25−28]

However, multilayers prepared by ESA usually present a low degree of internal organization. This may be a limitation of the technique, since well-organized multilayers are a prerequisite for a number of applications, including those requiring a vectorial transfer of energy, electrons, or matter or when the precise placement of active functional groups in confined layers is desirable.

The internal structure of multilayers obtained by ESA was investigated by a number of researchers. For multilayers assembled from one polyanion/polycation pair only, the interpenetration between successive "layers" is so important that no Bragg peaks are observed by grazing angle specular scattering measurements (X-ray reflectometry, XRR, or neutron reflectometry, NR), even when contrast is enhanced by selectively deuterating every second layer.[29−31] However, stratification was proved for multilayers containing more than two polyelectrolytes: $\{ABCB\}_n$, $\{(AB)_n(AC)\}_m$, $\{(AB)_n(AC)(AB)_m(AC)\}_p$ films have been assembled which give rise to Bragg peaks detected by XRR[32,33] and NR.[11,33−35] Furthermore, by selective deuteration at varying intervals along the film normal, the stratification of PAH/sulfonated polyaniline multilayers was also demonstrated to be preserved at least for the deposition of 40 bilayers.[30] Stratification of multilayers is also suggested by contact angle measurements showing odd/even trends as a function of the number of deposited layers.[36−39] Also, recent transmission electron microscopy (TEM) experiments by Rubner et al. clearly show stratification for multilayers of the $\{(AB)_n(AC)_m\}_p$ type, provided m and n are large enough.[40] These experiments indicate that the absence of Bragg peaks for normal two-components films is mainly due to an important interpenetration between neighboring layers, as demonstrated by a variety of other experimental techniques.[30,33,35−39,41−43] Hence, the name "fuzzy multilayers" was recently coined for such systems.[11]

Interpenetration can be reduced by using more rigid ionic blocks for the multilayer assembly. As a conse-

[†] Unité de physique et de chimie des hauts polymères.
[‡] Unité de chimie des matériaux.

10.1021/ma010092s CCC: $20.00
Published on Web 04/05/2001

quence, Bragg peaks may appear in X-ray measurements of some multilayers containing rigid inorganic platelets,[20,44−46] LB films,[47] bola-amphiphile[48,49] or colloidal nanoparticles.[50] However, even for these systems, the appearance of Bragg peaks is exceptional. For the sake of completeness, we mention that it was observed accidentally that a drying step applied at periodic intervals during multilayer buildup may induce sufficient contrast to give rise to Bragg peaks,[32] but very particular conditions seem to be necessary for that, as such structures could not be reproduced later on.[51]

Not only is the lack of structure detrimental to some applications, it also limits the information that can be obtained on polyelectrolyte (PEL) multilayers. Indeed, powerful techniques such as X-ray reflectometry, which are based on interferences between waves scattered at interfaces, are capable of providing detailed internal structural information only when at least partial order is present in the films. The situation somehow resembles the case of bulk materials, where material science strongly benefited early on from X-ray studies on crystalline materials, while knowledge of amorphous materials has lagged and still lags behind. As a result, progress in the understanding of mechanisms controlling PEL multilayer growth, and relationships between structure of multilayers and bulk complexes, are still badly needed.

In the present paper, we report on the growth and internal structure of PEL multilayers obtained by combining a specific ionene with different polyanions. As briefly mentioned in a series of previous publications,[52−55] this ionene may give rise to a high degree of internal organization when combined with the proper polyanions, as testified by the appearance of Bragg peaks in XRR measurements. In this paper, we present a detailed investigation of such multilayers, contrasting the results with those obtained on a "normal" standard ML based on poly(diallyldimethylammonium chloride) and poly(styrenesulfonate) (PDADMAC/PSS). In our conception, both types of multilayers grow by similar mechanisms, the differences between them resulting only from differences in the internal structure of the *bulk* polyelectrolyte complexes which can be formed. Therefore, our experiments on internally structured multilayers cast light on the growth behavior of PEL multilayers in general, without being limited to a relatively exotic class of multilayers. In a forthcoming paper, we will extend the results obtained in the present study to other polyelectrolyte systems, systematically varying the chemical structure of the ionenes.[56] Subsequent studies will deal with order in hybrid organic−inorganic multilayers.[57]

Experimental Section

Materials. a. Polyelectrolytes. The polyelectrolytes used in this study are shown in Figure 1. Ionene **1** is designated as I(*m*,R1,R2), where *m* is the number of methylene units in the chain backbone, R1 is a diammonium moiety (*N*,*N*,*N*′,*N*′-tetramethyl-1,5-diammonio)pentamethylene, NC_3N) and R2 is a pendent group (4-(pyridine-3yl azo)phenyl, PhN_2Pyr). The synthesis of ionene **1** I(10,NC_3N,ϕN_2Pyr) was described in ref 55. By elemental analysis, the degree of substitution of phenyl groups by the R2 moiety was determined to be 0.41. Poly(diallyldimethylammonium chloride) (PDADMAC, **2**), poly(vinyl sulfate) (PVS, **3**), poly(vinyl sulfonate) (PVSo, **4**), and poly(styrenesulfonate) (PSS, **5**) were purchased from Aldrich and used without purification. Poly(bis(3-sulfopropyl)itaconate) (PSPI, **6**) and poly(2-acrylamido-2-methylpropanesulfonate, sodium salt) (PAMPS, **7**) were described elsewhere.[58,59]

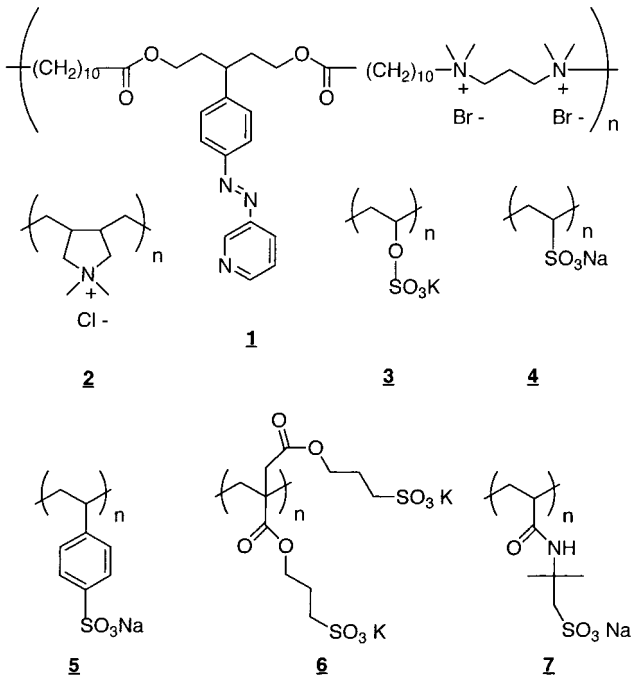

Figure 1. Chemical structure of the polyelectrolytes used in this study.

b. Substrates. One-side polished n-type ⟨100⟩ silicon substrates were purchased from ACM (France) and cut to get rectangles of 3 cm × 1 cm. Substrates were cleaned by immersion for 20 min in a hot 1:1 vol 98% H_2SO_4:27% H_2O_2 mixture ("piranha solution"; *caution*: piranha reacts violently with organic compounds and should not be stored in closed containers), followed by extensive rinsing with ultrapure water (obtained by deionization and purification using the Milli-Q system from Millipore). As was checked by XRR, this procedure efficiently removes organic contaminants without introducing measurable roughening of the surface. This procedure is known to produce a highly hydrophilic surface, leaving on the native layer of silicon oxide a relatively dense layer of silanols.[60,61] The presence of acidic silanol groups on the surface results in a globally negative surface charge density of the silicon surface in water. The thickness of the native oxide layer was estimated by ellipsometry on a series of clean wafers to be about 13 Å, with a standard deviation of 2 Å.

c. Multilayer Buildup. The cleaned substrates were dipped in a polycation solution for 10 min (unless otherwise specified), rinsed thrice by immersion in ultrapure water (3 × 1 min), then dipped for 10 min in a polyanion solution, and rinsed thrice. This deposition procedure was then cycled to obtain multilayers. The samples were air-dried at the end of their fabrication. For multilayers based on I(10,NC_3N,PhN_2-Pyr), the pH of the polyelectrolyte solutions was adjusted to 1 with hydrochloric acid. Unless otherwise stated, polycation and polyanion solutions were 2×10^{-2} M in charge (assuming protonation of 4-(pyridine-3-yl azo)phenyl for the polycation containing this pendent group). All solutions were prepared from ultrapure water and were used for not more than 48 h after preparation.

A special sample holder was designed in order to dip many samples simultaneously. Samples are successively removed from the sample holder after the desired number of dipping cycles. The growth of the multilayers is monitored from this set of samples, having all been synthesized under strictly identical conditions. This approach was selected because interrupting the deposition cycle several times for drying and measuring a given sample may disturb the deposition process.[6,62]

The nomenclature used in the following to design multilayers is as follows: A/{B/C}$_n$ indicates that *n* deposition steps were performed with B as polycation and C as polyanion,

starting from substrate A; A/{B/C}$_{n.5}$ indicates a similar deposition procedure, plus an extra deposition of polycation B.

d. Polyelectrolyte Complexes. Bulk polyelectrolyte complexes (or symplexes[63]) were simply obtained by mixing under vigorous stirring the polycation and polyanion solutions used for the preparation of the polyelectrolyte multilayers. After decantation, the solutions were filtered, and the complexes were collected and dried in air.

Characterization Techniques. a. Small-Angle X-ray Scattering (SAXS). SAXS was performed to obtain the long-range structure of symplexes (bulk polyelectrolyte complexes) and dry polyelectrolytes. SAXS was measured in transmission in an evacuated Kratky compact camera mounted on a Siemens rotating anode (Ni-filtered Cu Kα radiation, 40 kV/300 mA). A calibrated position-sensitive proportional counter (mBraun) was used to record the scattering patterns. Analysis of the data was performed either by directly fitting to the parasitic-corrected data theoretical models smeared to take into account the effects of beam shape and divergence[64] or by desmearing the parasitic and background-corrected signal using a variant of Glatter's algorithm[65] and using conventional analysis procedures. SAXS intensities are reported vs the length of the scattering vector, $s = (2/\lambda) \sin \theta$, where λ is the X-ray wavelength (1.5418 Å) and θ is half the angle between incident and scattered beams.

b. Wide-Angle X-ray Scattering. The experimental setup is based on a Siemens D5000 2-circles goniometer. X-rays of 1.5418 Å wavelength (Cu Kα) were obtained from a rotating anode. Monochromatization was achieved with the help of a secondary graphite monochromator, complemented with pulse height discrimination (scintillation counter). Soller slits placed in the incident and reflected beams limit axial divergence to 0.02°. Powder samples were deposited on silicon single crystals (large faces perpendicular to ⟨510⟩). Measurements were performed in reflection in an asymmetrical mode. The incoming angle of the X-ray beam on the silicon substrate was held fixed at 6°.

c. X-ray Reflectometry. The same goniometer as for WAXS studies was used for XRR. Proper collimation of the beam was obtained by using slits adjustable with micrometer precision. The vertical divergence of the incoming beam was typically 0.0084°. The vertical acceptance of the detector was fixed by a 200 μm wide slit placed at 20 cm distance from the sample. A special automated alignment procedure allowed to position the sample within a few micrometers from the goniometer center. More information on this setup can be found elsewhere.[66,67] XRR data were scaled to unit incident intensity and corrected for spillover at very low incoming angles (below ∼0.125°, depending on sample size and width of divergence slit). The data are reported as a function of K_{z0}, the component perpendicular to the interface of the wavevector in a vacuum of the incident photons (i.e., $K_{z0} = (2\pi/\lambda) \sin \theta$, where λ is the X-ray wavelength and θ is half the angle between the incident and reflected beams).

d. Ellipsometry. Two different commercial ellipsometers were used in this study: a L117 mechanical null ellipsometer from Gaertner (Chicago, US) and a Digisel rotating compensator ellipsometer from Jobin-Yvon/Sofie Instruments. Both ellipsometers are single wavelength ellipsometers, working at 6328 Å (He−Ne laser). For increased accuracy, two-zone measurements were performed with the L117 ellipsometer. To compensate some systematic errors (imperfections and residual misalignment of the optical components), measurements with the Digisel ellipsometer have been carried out with the analyzer at +45° and −45° (with respect to the plane of incidence).[68] Unless otherwise specified, a model consisting of an isotropic film on a flat substrate was used to fit the ψ and Δ measurements.[69] The refractive index of silicon was taken to be 3.881-j0.019.[70] When possible, the effective refractive index of the film was obtained from the ellipsometric measurements by fitting trajectories in the (ψ,Δ) plane corresponding to samples of increasing thickness, neglecting film absorption which is small at the working wavelength of the ellipsometer. Otherwise, the refractive index was arbitrarily fixed either to the refractive index of the most closely related system (when possible) or to 1.55. This latter value lies in the range of effective refractive indexes that were obtained experimentally on films containing the same polyanions and chemically similar polycations.[67] Furthermore, this refractive index is also in the range of refractive indexes of polymers in general.[71] The presence of an oxide layer atop the silicon substrate does not influence the effective index but results in an overestimation of the film thickness by about 15 Å.[72]

e. Miscellaneous. In-plane birefringence and dichroism of the films were studied in reflection with an AX70 Olympus optical microscope.[73] Birefringence and dichroism of the polycations and polyanions were studied in transmission. For these latter measurements, samples were prepared by evaporation of an aqueous solution of the polyelectrolyte on a glass substrate.

XRR Data Analysis. Given the importance of XRR results in this work, different analytical techniques were applied to the data:

First, for all samples, a Patterson function $P(r)$ was computed from reflectivity using[74]

$$P(r) = \frac{1}{2\pi} \int_{-\infty}^{\infty} \frac{R(K_{z1})}{R_F(K_{z1})} e^{2iK_{z1}r} \, dK_{z1} \quad (1)$$

where K_{z1} is the component perpendicular to the interface of the wavevector *in the film* and $R_F(K_{z1})$ is the Fresnel reflectivity of the bare and perfectly smooth substrate computed at K_{z1}. In the frame of the first Born approximation, i.e., kinematical theory, this function can be shown to be equal to the autocorrelation of the electron density gradient:[75]

$$P(r) = \frac{1}{\rho_s^2} \int_{-\infty}^{\infty} \frac{d\rho(z)}{dz} \frac{d\rho(z+r)}{dz} \, dz \quad (2)$$

where ρ_s is the electron density of the substrate and $\rho(z)$ is the electron density in the film at z, laterally averaged over the coherence area of the photons. This function presents a series of peaks located at r values corresponding to interdistances between interfaces in the film, positive peaks being associated with correlations between up/up or down/down interfaces and negative peaks with correlations between up/down or down/up interfaces. The width of each peak is proportional to the quadratic sum of the roughness of both interfaces being correlated, and its area is proportional to the product of electron density differences across both correlated interfaces. Because in our case the substrate/film interface is sharp and well-contrasted, $P(r)$ is often dominated by correlations between this interface and other interfaces, other cross-correlations being weaker. However, this may not be the case for the more regularly ordered multilayers, where the numerous cross-correlations between internal interfaces may dominate $P(r)$ near the origin. In addition, the failure of the first Born approximation near the region of total external reflection introduces a series of artifacts into $P(r)$. Nevertheless, the examination of $P(r)$ allows to rapidly obtain without a priori hypotheses information on film thickness, presence of internal electron density fluctuations in the film, internal repetition distance, and damping of order as a function of distance. These pieces of information may then be used, if so desired, for further analysis as described below.

Second, for samples displaying regular internal fluctuations of density, the method introduced by Singh et al.[76] was used to help determine the main features of the internal electron density fluctuations. However, this model was not capable to represent accurately the observed reflectivity over the whole K_{z0} range. We thus attempted to obtain refined pictures of electron density profiles by a so-called model-free fitting technique. The data were analyzed by fitting the parameters of a model representing the film as a succession of numerous thin virtual homogeneous layers with zero interfacial roughness. The film reflectivity was computed using dynamical theory.[77−80] The χ^2 function was minimized with a Marquardt−

Levenberg algorithm. To search parameter space, we mainly used a modification of the "delumping approach" proposed by Zhou et al.:[81] The number of virtual layers was progressively increased until the thickness of all virtual layers was smaller than $2/K_{z0,max}$. To avoid numerical problems and unphysical solutions due to the large number of parameters in the final model of the electron density, a regularization technique was applied by adding a smoothing constraint to the χ^2 function.[79,82] The selected constraint was

$$C = \sum_k (\rho_{k+1} - \rho_k)^2 \quad (3)$$

where ρ_k is the electron density of the kth layer of the model. The constraint was multiplied by a Lagrange parameter, whose optimal value was found by performing the fitting procedure for different values of this latter coefficient: The optimal value leads to the largest decrease of the constraint term without significant increase of the χ^2 function. Values in the range 5000−10 000 were usually found to be optimal. Further details on the fitting routine can be found elsewhere.[67]

Results

Classical System Based on PDADMAC/PSS. For purposes of comparison, we first present the growth behavior of "classical" multilayers made of two strong polyelectrolytes. Figure 2a shows X-ray reflectograms obtained for a series of multilayers of increasing thickness made from poly(diallyldimethylammonium chloride) and poly(styrenesulfonate) (PDADMAC/PSS). Above 3.5 deposition cycles, Patterson functions (Figure 2b) display a clear peak being displaced to longer distances with number of deposition cycles, indicating regular film growth. This peak represents correlations between substrate/film and film/air interfaces. Below 3.5 deposition cycles, only a broad bump is detectable in the Patterson functions, indicating that no real film can be defined since thickness is too small vs multilayer and/or substrate roughness. This is confirmed by an inspection of electron density profiles (Figure 2c), where it can indeed be checked that no density plateau associated with a film is apparent below 3.5 deposition cycles. Below this value, only a relatively rough deposit is detectable in the density profiles. For larger numbers of deposition cycles, a film is clearly detected, its thickness increasing regularly with dipping cycle.

The variation of film thickness vs number of deposition cycles (n_{cycl}) is reported in Figure 2d. For $n_{cycl} \geq 3.5$, the thickness can be defined unambiguously and determined from the location of the last peak in the Patterson functions (black squares). For smaller values of n_{cycl}, different average thickness may be defined for the deposits depending on the measurement technique used. We have estimated thickness (d) by XRR, from the location in reciprocal space of the first minimum of reflectivity using $d = \pi/2/K_{z1,min}$, where $K_{z1,min}$ is the component of the wavevector of the photons *in the film*, corresponding to the first minimum of reflectivity, in the direction of substrate normal. $K_{z1,min}$ was computed applying a refraction correction[83] using 0.37 Å^{-3} as average film electron density, which is the value found for thicker films by the fitting procedure; it should be realized that this refraction correction is only important for the thicker films. A good agreement is found between the thickness defined from Patterson functions and from $K_{z1,min}$, for samples for which both can be determined. Alternatively, we used ellipsometry to obtain an average film thickness using 1.5 as average refractive index for the deposits. The ellipsometric thickness are systematically larger by about 12 Å compared to the values obtained by the two XRR determinations, due to inclusion of the silicon oxide layer thickness in the ellipsometric thickness.[72]

Thickness evolves linearly with the number of deposition cycles, with an increment of about 4 Å per deposition cycle.[84] This value is very small; previous measurements on the same pair of polyelectrolytes provided as increment per deposition cycle 20−30 Å for solutions 0.5 M in NaCl[85] and 24.5 Å for solutions 0.1 M in NaCl.[86] Others reported a growth increment of 4.1 Å for PSS/poly(allylamine hydrochloride) multilayers grown at pH 4.[87] As thickness increments vary according to the square root of salt concentration,[88] our results agree reasonably with available data. This small increment obviously excludes considering the film as a neat succession of flat layers of PDADMAC and PSS. In addition, our results clearly show that the first adsorption steps do not lead to flat thin films but to deposits of roughness larger than the one of the substrate (Figure 2e). A detailed comparison of density profiles indicates that, initially, the amount of material deposited is larger upon PDADMAC adsorption than upon PSS adsorption (Figure 2e). This however does not hold anymore true for larger numbers of dipping cycles (Figure 2f).

Figure 2e−f provides unique views of film growth, illustrating the slight increase of roughness during film growth and the clear fact that films cannot be considered true multilayers. Given the extensive body of results that can be found in the literature on similar systems,[15] we will not elaborate further on these results.

Ordered System Based on I(10,NC_3N,PhN_2Pyr)/PVS. a. Growth of Multilayers. Figure 3 presents the evolution of thickness vs number of deposition cycles for samples prepared with 2, 10, and 20 min dipping times. The growth is linear, with 88 Å average increment per deposition cycle, except for the very first deposition cycles (inset of Figure 3). This deviation from linearity at small numbers of dipping cycles was reported before for many pairs of PEL's.[15] It must be traced back to the perturbing influence of the substrate.[89] Shorter deposition times result in slightly smaller thickness and larger scattering of the data. Both XRR and atomic force microscopy (AFM) agree reasonably in indicating a small progressive increase of roughness with ongoing deposition, with rms roughness varying between 5 and 40 Å following sample.

By performing experiments where growth was stopped every half-cycle of deposition, we determined by ellipsometry that the average thickness increment (in the linear region) per ionene adsorption amounts to 66 Å (with a standard deviation of 9 Å determined on six samples), while the thickness increment corresponding to PVS adsorption is 24 Å (with a much larger standard deviation). From the computed[90] molar volumes of I(10,-NC_3N,PhN_2Pyr) (660 cm^3) and PVS (70 cm^3), assuming full charge compensation between polycation and polyanion (i.e., exclusion of small counterions from the films), one may compute from the total increment per bilayer of 88 Å, a PVS increment of 18 Å, and a I(10,-NC_3N,PhN_2Pyr) increment of 70 Å, in rather good agreement with the direct determination. This confirms that the growth of the multilayer is mostly controlled by charge compensation mechanisms, with exclusion of most small counterions.[86]

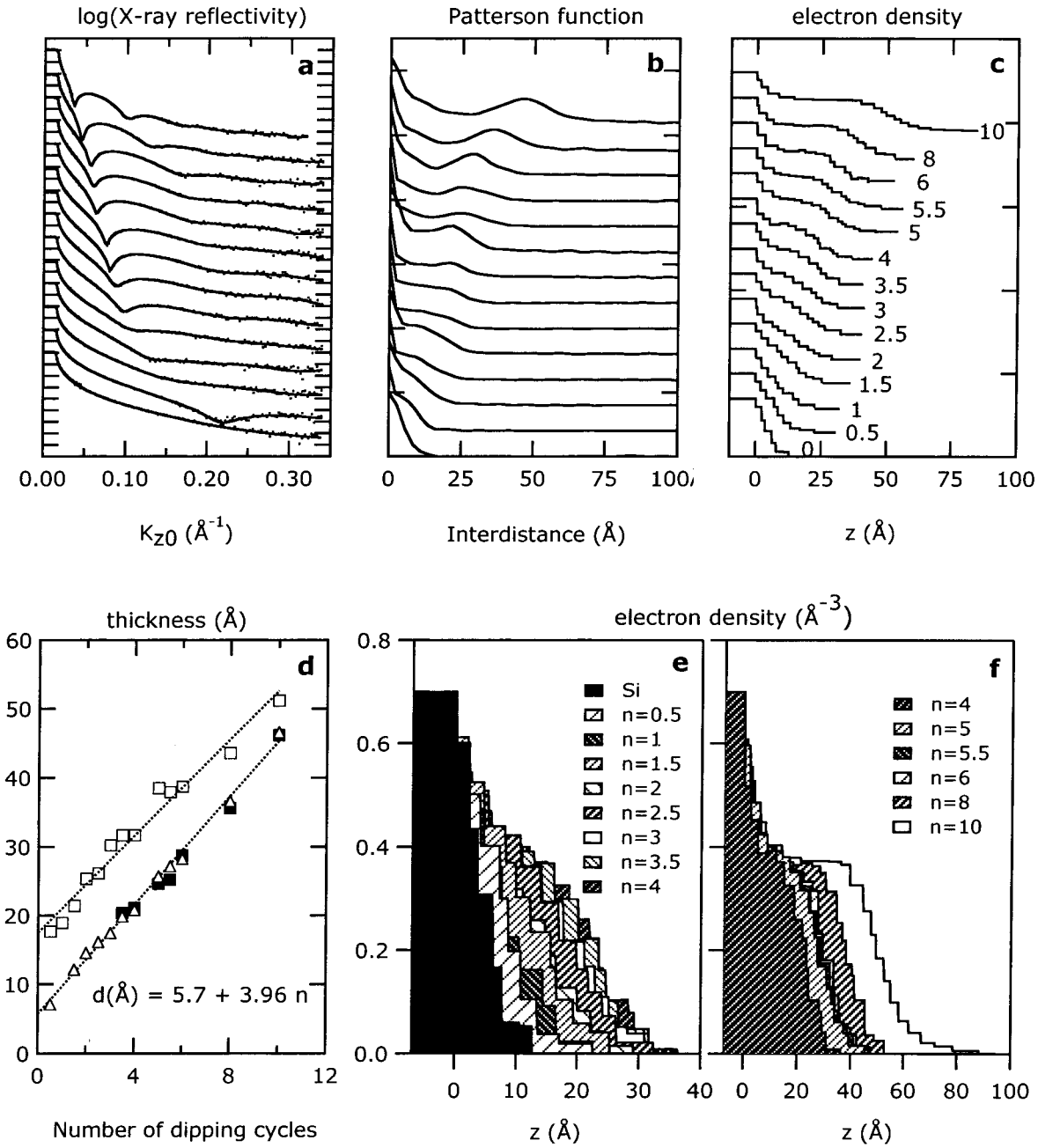

Figure 2. (a**)** X-ray reflectivity of Si/{PDADMAC/PSS}$_n$ multilayers with, from bottom to top, n = 0, 0.5, 1, 1.5, 2, 2.5, 3, 3.5, 4, 5, 5.5, 6, 8, and 10. Curves are displaced vertically for clarity. Dots are experimental data; continuous lines are fits using density profiles of (c). (b**)** Patterson functions computed from the data of (a). Traces are displaced vertically for clarity and are drawn in the same order as in (a). Patterson functions are normalized to unity at the origin. (c**)** Electron density profiles obtained by model-free fitting of the reflectivity data of (a). Traces are displaced vertically for clarity and are drawn in the same order as in (a). (d**)** Variation of sample thickness vs number of deposition cycles for Si/{PDADMAC/PSS}$_n$ multilayers. Thickness determined by ellipsometry (open squares), analysis of Patterson functions (filled squares), or direct analysis of the XR reflectograms (triangles). The lines are fits to the data. (e, f) Detailed comparison of electron density profiles of Si/{PDADMAC/PSS}$_n$ multilayers. Symbols are given in figures. Electron densities are normalized to 0.7 Å^{-3} in the substrate, to suppress small vertical fluctuations of the profiles resulting from minor alignment problems.

b. Internal Structure of the Multilayers. Figure 4 presents X-ray reflectograms (top) of selected Si/{I-(10,NC_3N,PhN_2Pyr)/PVS}$_n$ multilayers prepared with 10 min dipping time, together with their associated Patterson functions (bottom). Numerous sharp Kiessig fringes on the reflectograms testify for the limited roughness of both film interfaces. The translation of Kiessig fringes in the Patterson function is the final peak which is progressively displaced toward larger interdistances as film thickness increases. This peak is less easily perceptible for thicker films, because of its broadening due to increasing roughness and because Patterson functions are normalized to unity at zero interdistance.

The most interesting and unusual feature of the reflectograms is the presence of a sharp (Bragg) reflection at about 0.135 Å^{-1}, corresponding to repetition distances of about 23.5 Å. In addition, a dip in the reflected intensity is clearly detectable for thicker samples at the location expected for the second-order Bragg peak. These features translate into a regular oscillation in the Patterson functions, starting from zero

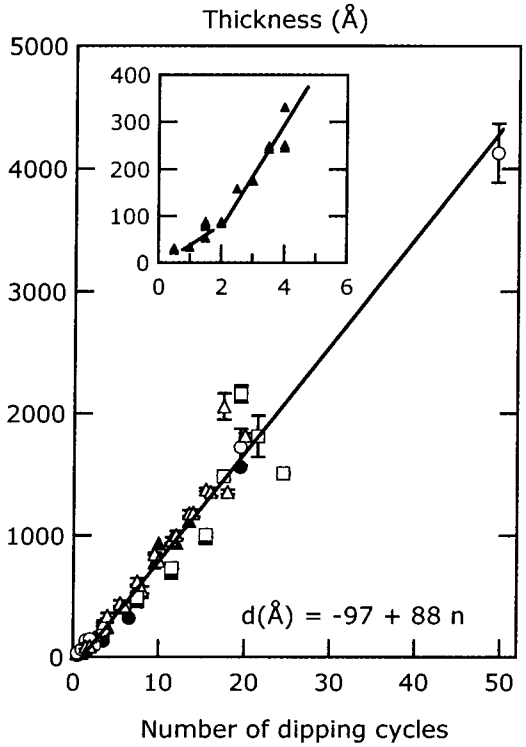

Figure 3. Thickness vs number of deposition cycles for multilayers based on I(10,NC_3N,PhN_2Pyr)/PVS. Dipping times: 2 min (squares), 10 min (triangles), 20 min (circles). Filled symbols: thickness determined by XRR; open symbols: thickness determined by ellipsometry. The line is a linear regression through all data points. Inset: zoom on the region of initial growth, showing deviation from linearity. Lines are drawn as support to the eye.

up to the peak of total thickness. It is obvious from these data that the multilayers are internally structured, with a regular lamellar fluctuation of electron density starting from the substrate and extending deep into the film.

A first question which arises is the distance over which this regular oscillation extends in the film. An answer to this question may be obtained by performing a Debye−Scherrer analysis[91] of the line width of the first Bragg peak. Figure 5 shows the so-obtained number (N_{DS}) of repeat periods in the film vs film thickness. For thickness lower than 800 Å, the regular fluctuation extends over the whole film thickness (theoretical line in Figure 5).[92] For thicker films, the number of oscillations found in the film saturates at a value of about 35−45.

N_{DS} is actually a measure of the size of coherently diffracting regions, with electron density fluctuations being integrated laterally over the coherence area of photons (in the range of μm^2 given our collimation conditions). The saturation of N_{DS} does not necessarily signify that no regular lamellar fluctuation of electron density is present in the film farther than 800 Å from substrate. It may be simply due to a loss of vertical correlations between any two lamellae separated by more than 800 Å, due to cumulating irregularities in the interlamellar distances ("paracrystalline" vertical stacking[93]) or to increasing roughness of the lamellae as one moves further away from the substrate, resulting in the smearing and eventual disappearance of the lamellar fluctuation in the laterally averaged density profile.

The following experiments indicate that both explanations hold true for our films. A 24.5 bilayer sample

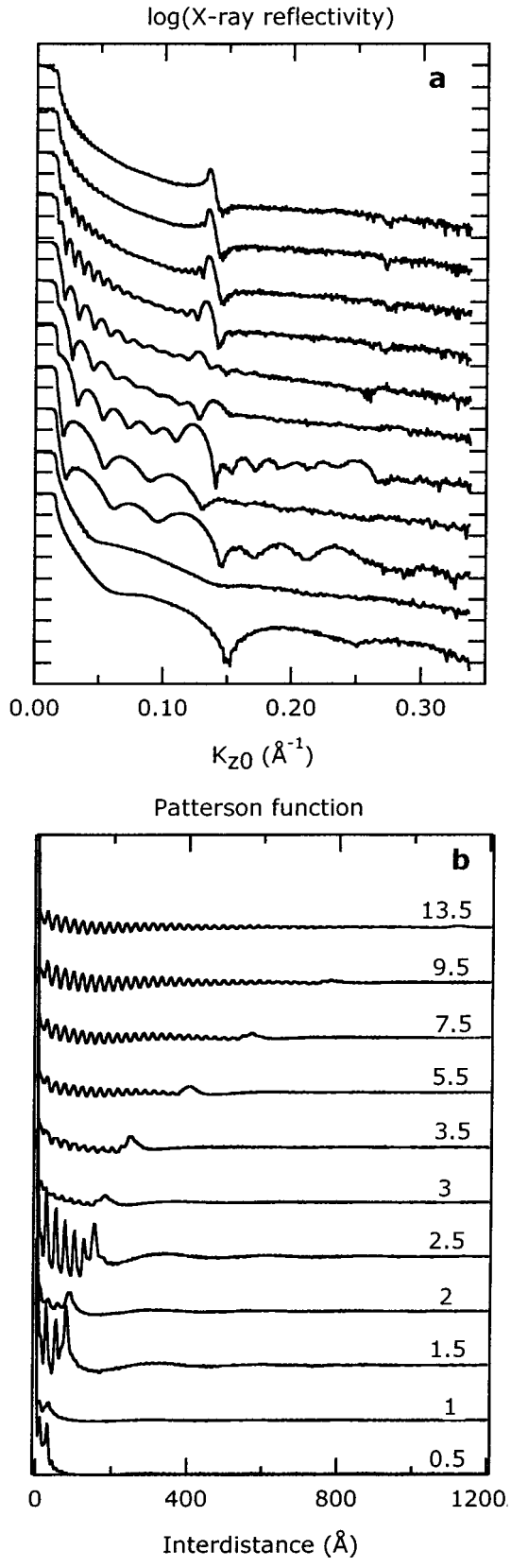

Figure 4. (top) X-ray reflectivity of selected Si/{I(10,-NC_3N,PhN_2Pyr)/PVS}$_n$ multilayers prepared with 10 min dipping time. Curves are displaced vertically for clarity. (bottom) Patterson functions computed for the same samples. Curves are displaced vertically for clarity. Patterson functions are normalized to unity at the origin. From top to bottom: n = 13.5, 9.5, 7.5, 5.5, 3.5, 3, 2.5, 2, 1.5, 1, and 0.5 cycles of deposition.

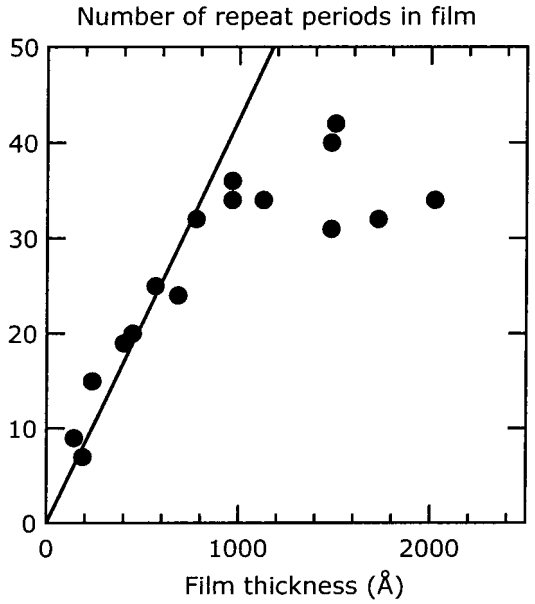

Figure 5. Number of periods of oscillation of electron density in the multilayers vs film thickness. Data obtained from Debye−Scherrer law. The line corresponds to regular oscillations extending over whole film thickness.

(Si/{I(10,NC_3N,PhN_2Pyr)/PVS}$_{24.5}$) was grown using a short dipping time of 2 min. X-ray reflectivity was measured, and a series of longitudinal diffuse scans were obtained (i.e., with the scattering vector tilted from sample normal, inset of Figure 6a). Figure 6a,d shows diffuse scans and specular reflectivity for this sample (sample 1). As can be observed, the diffuse off-specular scattering is rather important for this sample, compared to specular. Application of the Debye−Scherrer law leads to $N_{DS} = 31$. Then, the sample was immersed into ultrapure water at 40 °C for 36 h, dried, and measured again. Figure 6d (sample 2) shows that a second-order Bragg peak then emerges in the reflectogram, while specular scattering increases relative to the diffuse one (Figure 6b). In addition, N_{DS} increases to 40. As diffuse scattering results from the roughness of lamellae (or from local tilting of these lamellae vs the surface of the substrate), this experiment demonstrates that roughness of the lamellae indeed plays a role in the limitation of N_{DS}.

However, the saturation of N_{DS} does not result only from internal roughness. Figure 6c,d presents diffuse scans and specular reflectivity for a 19.5 bilayer sample grown with longer (20 min) dipping time (sample 3). In this case, up to four Bragg peaks are observed in the reflectogram, while specular scattering increases tremendously compared to diffuse scattering, although N_{DS} increases only to 48. For this specific sample, it is possible to extract more information on internal disorder from the multiple orders of reflection. According to Hosemann's theory of paracrystallinity,[93] ΔK_{z0}, the full width at half-maximum of the nth Bragg reflection, is related to the number of coherently diffracting lamellae (N_H) by

$$\Delta K_{z0}/(0.888K_{z0,1}) = 1/N_H + (\pi g n)^2 \qquad (4)$$

where $K_{z0,1}$ is the value of K_{z0} at the first Bragg peak, and g is the relative standard deviation of the repeat period due to irregularities in the interlamellar distances. This relationship is displayed in the inset of Figure 6d, from which we obtain $N_H = 59$ and $g = 0.019$. This indicates that the variation of interdistances between two successive oscillations in the laterally integrated electron density profile amounts to about 2%; the progressive accumulation of such random irregularities leads to a total variation of about one repeat period for two lamellae separated by about 50 other oscillations, leading to loss of vertical coherence of the packing over such distances. Hence, it should therefore not be concluded that layering does not exist over the whole film thickness; instead, *local* ordering most probably persists up to the air interface for all films.

These experiments also indicate that multilayers can be internally perfected by proper annealing in water, which suggests considerable water diffusion and local mobility of chain segments in the films. Furthermore, it becomes evident that the initial multilayers are far from equilibrium, being trapped in a more disordered state.

A second question immediately arises when considering Figure 4. As the internal repeat period is about 23.5 Å, while the increment of thickness amounts to 88 Å per deposition cycle (Figure 3), the inescapable conclusion follows that 3−4 repeat periods are deposited per dipping cycle. This is strictly valid, since we just demonstrated before that films are fully filled with lamellar layers. To understand this, we followed in detail the initial steps of growth of the multilayer by XRR, as shown in Figure 7. After a single adsorption of the ionene, both density profile and Patterson function indicate that some electron density fluctuation already exists into the adsorbed layer, which suggests prestructuring of the ionene layer. Subsequent adsorption of PVS results in a limited thickness increase. Importantly, the addition of PVS also results in density being modified inside the region coinciding with the previously deposited ionene layer (Figure 7, bottom). This shows that PVS diffuses into the previously adsorbed ionene layer, promoting reorganization through I(10,NC_3N,PhN_2-Pyr)/PVS complexation. This is fully supported by the comparison of the two successive Patterson functions, which indicates a change of contrast inside the multilayer upon PVS addition. Also, note the important width of the film/air interface.

Upon readsorption of the ionene (Figure 7, bottom), the multilayer thickness increases significantly, with the addition of two new oscillations in the electron density profile. These oscillations appear at locations previously corresponding to the broad film/air interface, suggesting considerable diffusion of the ionene in the previously adsorbed film, with concomitant surface-constrained complexation occurring. Further addition of PVS leads to a slight thickness increase, diffusion of PVS in the previously adsorbed film, and limited reorganization of the previously adsorbed layers, as testified also by the variations of contrast detected in the Patterson functions. This process goes on upon further adsorptions.

Also, the alternation of the quality of the structure is clearly visible in Figure 7. After ionene adsorption, the amplitudes of Bragg peaks in reflectograms and of the oscillations in the Patterson functions are strong. Upon PVS adsorption, these amplitudes strongly decrease, showing unambiguously that PVS penetrates the film upon adsorption and destroys partially the previous ordering.

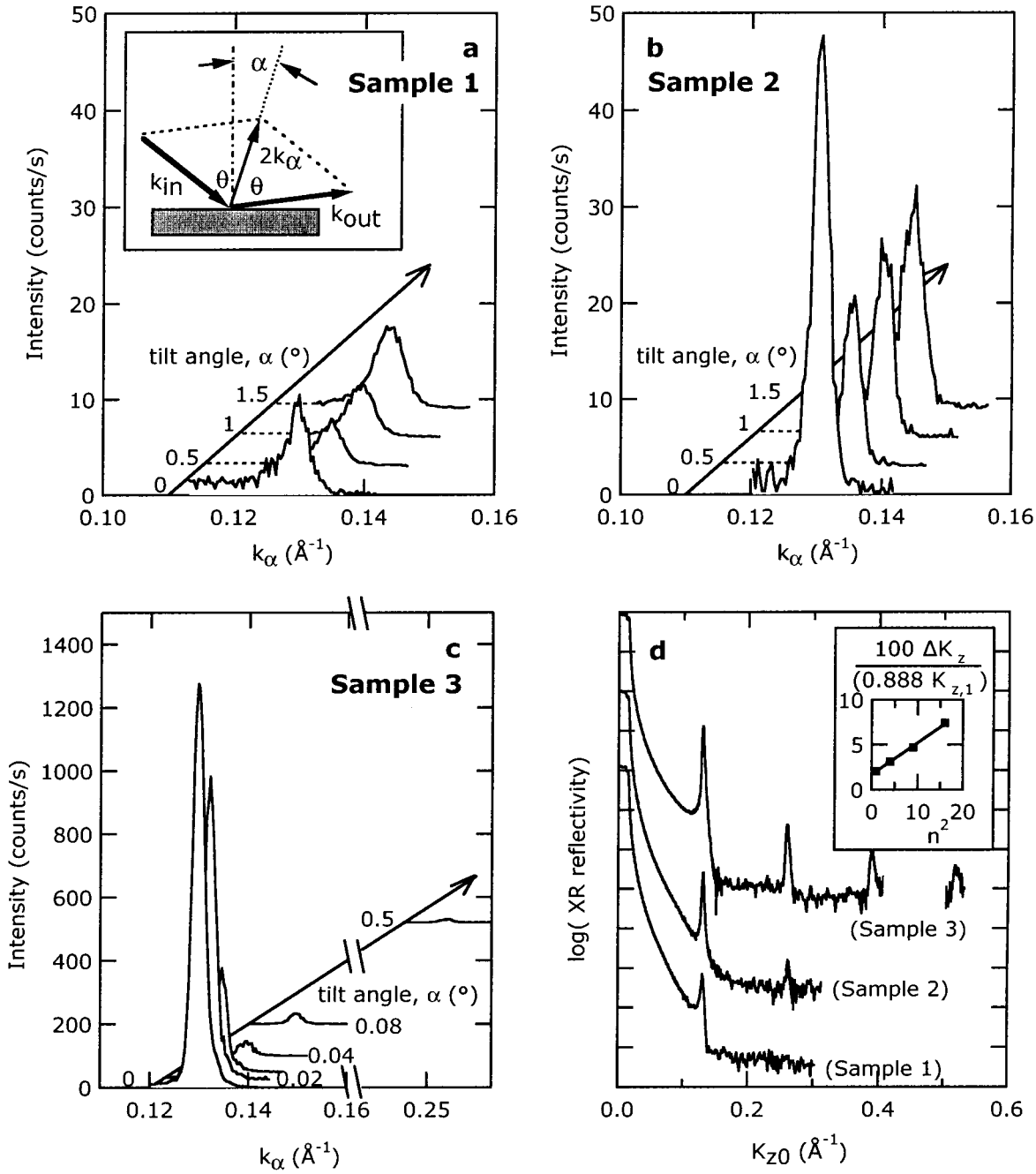

Figure 6. (a) Longitudinal diffuse scans of a Si/{I(10,NC_3N,PhN_2Pyr)/PVS}$_{24.5}$ sample grown using a short dipping time of 2 min (sample 1). The geometry of the scattering is displayed in the inset of this figure. $2k_\alpha$ is the length of the scattering vector, inclined at an angle α from sample normal. (b) Longitudinal diffuse scans of the same sample as in (a) after 36 h annealing into water at 40 °C (sample 2). (c) Longitudinal diffuse scans of a Si/{I(10,NC_3N,PhN_2Pyr)/PVS}$_{19.5}$ sample grown with 20 min dipping time (sample 3). Note the extremely sharp decrease of Bragg intensity with tilt angle. **(**d) X-ray specular reflectivity of samples 1, 2, and 3 of Figure 6a−c. Inset*:* variation of Bragg peak width for sample 3 vs square of reflection order.

From this set of experiments, it readily appears that internal structure (i.e., internal repeat period) and growth (i.e., thickness increment per adsorption) are two unrelated concepts. As shown previously, increments are governed by charge balance considerations. Internal structure results from the intrinsic trend of I(10,-NC_3N,PhN_2Pyr) to form structured adsorbed layers and surface-constrained complexation between PVS and the ionene occurring upon diffusion of the next adsorbed polyelectrolyte into the previously adsorbed film. Depending on the amounts adsorbed, this will give rise to a specific number of oscillations (or lamellae) being added per dipping cycle.

c. Structure of Bulk Ionene and I(10,NC_3N,-PhN_2Pyr)/PVS Complex (Symplex). The validity of the previous explanation rests on the existence of a specific complexation mechanism between I-(10,NC_3N,PhN_2Pyr) and PVS, giving rise to ordered samples. Bulk I(10,NC_3N,PhN_2Pyr) is a semicrystalline polymer displaying typical spherulites when viewed by optical microscopy between crossed polarizers and presenting sharp WAXS reflections.[67] This polymer also exhibits a small-angle sharp Bragg reflection at 28 Å, resulting from some long-range organization of the polymer in the bulk, probably due to microphase separation between the long hydrophobic segments and the

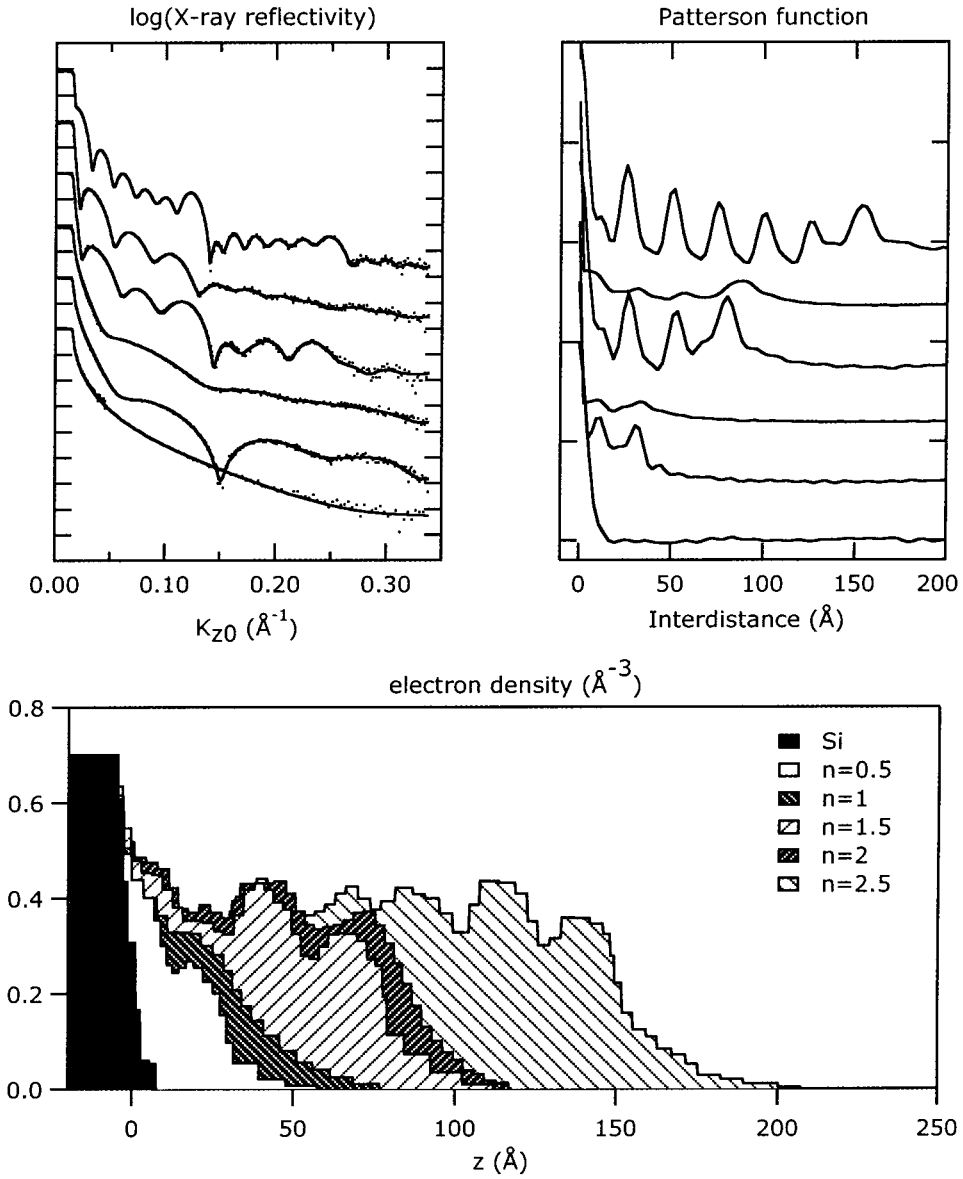

Figure 7. (top left) X-ray reflectivity of Si/{I(10,NC_3N,PhN_2Pyr)/PVS}$_n$ samples, with n = 0, 0.5, 1, 1.5, 2, and 2.5 (from bottom to top). Curves have been displaced vertically for clarity. Dots: experimental data. Continuous line: fits using the density profiles presented below. (top right) Patterson functions of same samples. Curves have been displaced vertically for clarity. Patterson functions are normalized to unity at the origin. (bottom) Electron density profiles obtained from the model-free fits to the experimental reflectivity. Electron densities are normalized to 0.7 Å^{-3} in the substrate, to suppress small vertical fluctuations of the profiles resulting from minor alignment problems.

polar groups.[67] Concentrated aqueous solutions of this ionene are birefringent, indicating that I(10,NC_3N,PhN_2-Pyr) forms a lyotropic mesophase. This certainly is the reason for the prestructuring of the first adsorbed ionene layer, which was detected above.

Coprecipitation of PVS and I(10,NC_3N,PhN_2Pyr) leads to the formation of an insoluble symplex, whose stoichiometry is governed by charge balance between polycation and polyanion, as was determined by infrared spectroscopy and elemental analysis.[67] WAXS indicates the symplex not to be crystalline. However, the symplex presents a clear lamellar superstructure, with a repeat period of about 24 Å, as revealed by SAXS (Figure 8). The lamellar organization perfects upon annealing the sample for a few days in water. This is obvioulsy reminiscent of the behavior of multilayers based on the same polyelectrolytes, including the value of repetition distance. Fit of the general paracrystalline model of Hosemann[93] to the annealed sample (Figure 8) indicated that the complex structure is based on lamellar regions of about 15.4 Å separated by lamellar regions of about 9.2 Å thickness, of different electron density. Broadening of the reflections results from paracrystalline disorder. Clearly, the complex is well-organized at the supramolecular level, with probably microphase separation occurring between hydrophobic, less electron-dense regions of I(10,NC_3N,PhN_2Pyr) and more electron-dense regions containing the sulfate groups of PVS. The very same complex is formed in the multilayers. Differences between complex in multilayers and bulk lie in the degree of preferential orientation and probably in the rate at which complexation occurred.

d. Experiments Performed on I(10,NC_3N,PhN_2Pyr) Combined with Other Polyanions. Given the internal ordering of the multilayers results from specific complexation between the ionene and PVS, it was tempting to investigate the effect of counterpolyanions on the structure of the multilayers and the bulk

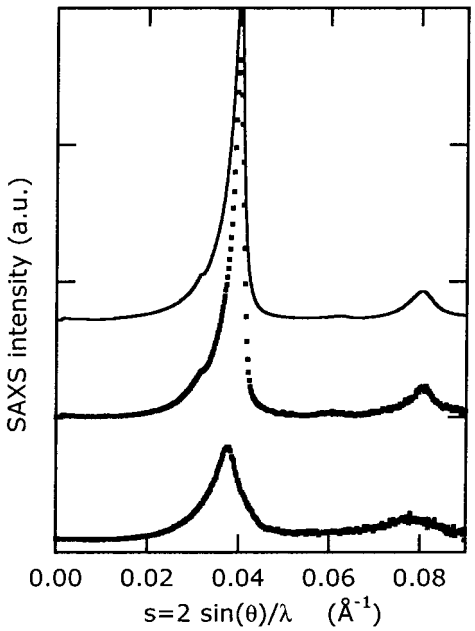

Figure 8. Small-angle X-ray scattering of I(10,NC_3N,PhN_2-Pyr)/PVS bulk complex. Intensities (not desmeared) have been multiplied by s^2 to facilitate curve inspection. Bottom curve: experimental data, complex as precipitated; middle curve: experimental data, previous sample annealed for a few days in water; top curve: fit of the general paracrystalline model of Hosemann to the data, taking into account smearing due to beam shape and divergence. All curves are displaced vertically for clarity.

complexes. Figure 9 shows that ordered multilayers are obtained when using poly(vinyl sulfate) (repeat period of 24 ± 1 Å) or poly(vinyl sulfonate) (repeat period of 22.4 ± 1 Å) as polyanion. In addition, the Patterson function of multilayers grown with PSPI as polyanion displays weak oscillations superimposed on a broad bump, indicating that such multilayers are extremely rough, with a slight internal density modulation with a repeat period of about 33 ± 3 Å. Small-angle X-ray scattering of the coprecipitated polyelectrolyte solutions (Figure 9, right) confirms that these three polyanions indeed form structured complexes when combined with the ionene. After desmearing and Lorentz correction, repeat distances of 24, 25, and 32.5 Å are found for the complexes made from PVS, PVSo, and PSPI, respectively,[94] in relatively good agreement with the values found in the multilayers.

By contrast, there is no evidence from SAXS for internal structuring of bulk complexes made from I(10,-NC_3N,PhN_2Pyr) and either PAMPS or PSS. Accordingly, multilayers grown with these two polyelectrolytes are also unstructured, PAMPS giving rise to relatively smooth multilayers (displaying a single sharp peak in the Patterson function), while PSS only provides very rough multilayers characterized by a broad bump in the Patterson function. Hence, we may safely conclude at this stage that the ability of the polycation and polyanion to give rise to structured complexes is one of the reasons explaining the appearance of order into the multilayers, thereby confirming that surface-constrained complexation plays an important role in multilayer structuring. However, the situation is actually more complicated, as will be shown in a sequel to this paper.[56]

e. Preferential Orientation in I(10,NC_3N,PhN_2-Pyr)/PVS Multilayers. As shown above, the lamellae in the multilayers may be very well aligned with respect to the substrate (cf. Figure 6c), provided proper deposition conditions are selected. One would expect that such ordering might lead to preferred orientation of selected chain fragments in the multilayer. Since the ionene bears a chromophore, one could expect to get uniaxial optical properties, with the unique axis being perpendicular to the substrate. We fitted an isotropic model, as well as an uniaxial model,[69] to the ellipsometry data obtained on a series of I(10,NC_3N,PhN_2Pyr)/PVS multilayers grown with 10 min dipping time. The results in Figure 10a indicate that the uniaxial model fits much better the set of ellipsometric data points. In addition, thickness obtained from the uniaxial model agree better with XRR-determined thickness (Figure 10b). An ordinary refractive index n_0 (i.e., parallel to the film surface) of 1.53 ± 0.01 and an extraordinary refractive index n_e (i.e., along the normal to the sample surface) of 1.63 ± 0.03 are deduced from the uniaxial fit. This strongly suggests preferential orientation of the more polarizable chromophore side groups along the sample normal.

f. Reproducibility. Different series of samples were prepared from different solutions of different batches of the ionene synthesized at different occasions and were measured over a period of 3−4 years. Growth of the multilayers was found to be rather reproducible, as can be checked from Figure 3 which presents the whole set of thickness data acquired over this period of time. Preferential orientation was found to vary slightly over three different series of samples, with n_0 = 1.53, 1.54, 1.53 and n_e = 1.65, 1.66, 1.63, respectively. The location of the first-order Bragg peak varied slightly, corresponding to repeat periods between 23.3 and 24.5 Å. The main variability between successive experiments was in the height and width of Bragg reflections, indicating variable degree of order in the multilayers depending on (sometimes uncontrolled) details of the deposition conditions.[67] A few depositions were performed on quartz instead of silicon or on silicon primed with a buffer layer of poly(ethylene imine)/poly(vinyl sulfate). These multilayers were not significantly different from others.

Discussion

The previous set of experiments clearly show that it is possible to obtain highly ordered polyelectrolyte films, consisting of a regular lamellar nanostructure extending over considerable distances in the films. Lamellae may lie flat on the substrate within better than 0.08°, resulting in preferential orientation of specific chain fragments in the film. This is the first PEL system reported to date to exhibit such characteristics, opening new perspectives for applications requiring preferential alignment or strict confinement of active groups in layers.

Perhaps more importantly, this system allowed us to perform a detailed analysis of film growth and to directly compare film internal structure with the structure of bulk complexes. From this analysis, we conclude that three mechanisms govern film growth and structuring: adsorption, diffusion, and complexation. Indeed, the results show that (1) the amount of polyelectrolyte adsorbed on the film (thickness increments) is controlled by charge balance, (2) the adsorbed PEL does not form a neat layer over the growing film, but instead diffuses into the film over some finite distance, and (3) the mixing occurring through this diffusion process results in complexation of polyanion and polycation (and most

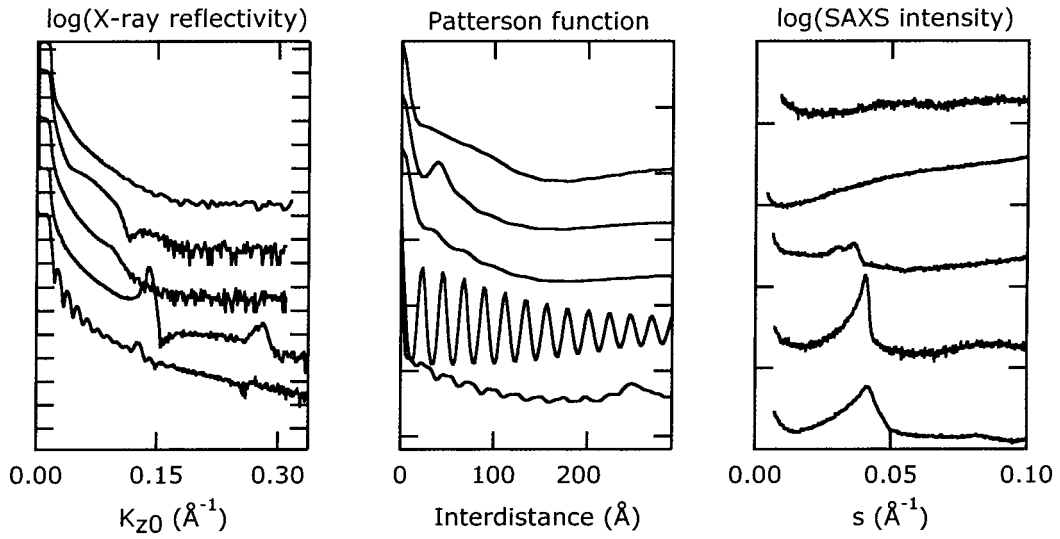

Figure 9. (left) X-ray reflectivity of Si/{I(10,NC_3N,PhN_2Pyr)/polyanion}$_n$, where (polyanion,n) = (PVS,3.5), (PVSo,6), (PSPI,4), (PAMPS,4), and (PSS,4), from bottom to top. Curves are displaced vertically for clarity. (middle) Patterson functions corresponding to the samples of left figure. Curves are displaced vertically for clarity. Patterson functions are normalized to unity at the origin. (right) SAXS of bulk complexes obtained by coprecipitating a solution of I(10,NC_3N,PhN_2Pyr) with a solution of, from bottom to top, PVS, PVSo, PSPI, PAMPS, and PSS. SAXS intensities are raw intensities and are displaced vertically for clarity.

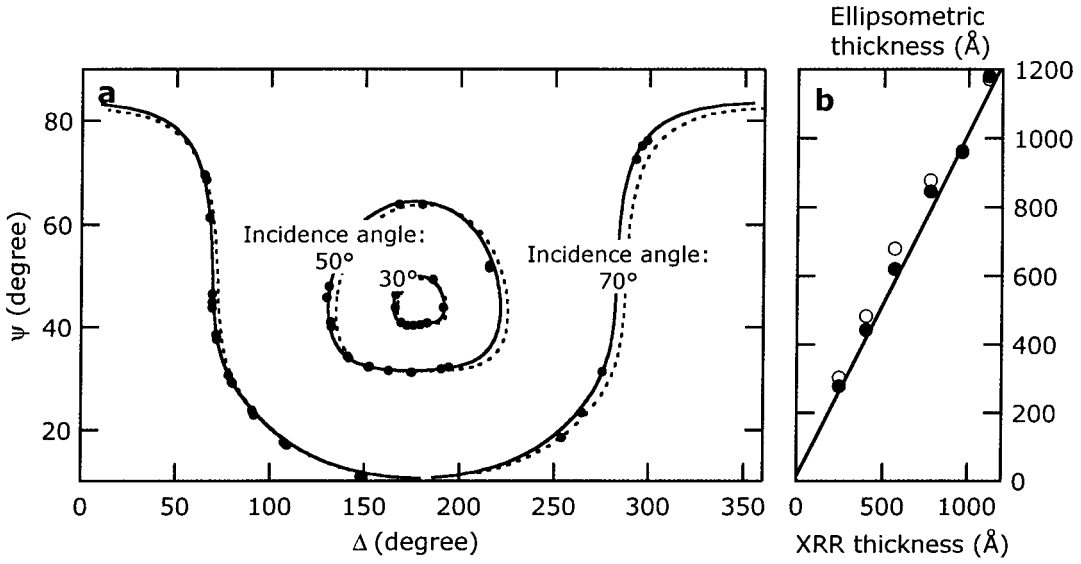

Figure 10. (left) Ellipsometric angles determined on a series of I(10,NC_3N,PhN_2Pyr)/PVS multilayers grown with 10 min dipping time (filled circles). Measurements were performed for three incidence angles. Dashed lines: ellipsometric trajectories drawn for increasing sample thickness, computed from optical parameters determined by fitting an isotropic model to the experimental data. Continuous lines: ellipsometric trajectories drawn for increasing sample thickness, computed from optical parameters determined by fitting an uniaxial model to the experimental data. (right) Plot of film thickness as obtained by ellipsometry vs film thickness determined by XRR. Open symbols: optical parameters determined by fitting an isotropic model to the experimental data; filled symbols: optical parameters determined by fitting an uniaxial model to the experimental data. The uniaxial model reduces the discrepancy between ellipsometry- and XRR-determined thickness.

probably ejection of most small counterions from the film, as shown by others[86]). If polyanion and polycation are capable of forming structured symplexes, complexation may lead to internal structuring of the film, as for I(10,NC_3N,PhN_2Pyr)/PVS. Constraints set by the rigid wall nature of the substrate will force preferential orientation of structural features (e.g., lamellae), as observed. If, by contrast, polyanion and polycation can only form "scrambled egg" types of symplexes,[95,96] then a "classical multilayer" will ensue, with no real layering of polyelectrolytes.

These three mechanisms, which occur almost simultaneously, may explain the growth of both unstructured and structured PEL films and allow to understand how increments of thickness per deposition cycles as small as 4 Å can be achieved. It also explains why more than one repeat period may appear per dipping cycle for structured systems such as I(10,NC_3N,PhN_2Pyr)/PSS. In addition, previously published data on PEL film growth agree with this model. The importance of complex formation in film growth was already suggested by Schlenoff et al.;[86,97] the scrambled egg nature of this complex for usual multilayers was implicitly recognized by Rubner et al.,[39,98,99] who described PEL self-assembled films as molecular-level blends of PEL's. Our results provide direct experimental support to these views. In this respect, it should be emphasized that the word "multilayer" is improperly used to design PEL films; one should better designate them as "electrostatic self-assemblies" or "PEL molecular-level blends".

This does not mean that electrostatic self-assemblies are not stratified. Diffusion of polyelectrolytes in the film upon adsorption is certainly restricted to short distances, as shown by many experiments by previous workers (see Introduction).[11,32−40] But stratification may only exist for length scales larger than the increment of thickness per deposition cycle. At the scale of the layer pair, there is no net separation between polyanion and polycation. Recently, Decher et al. proposed a structural model for electrostatic self-assemblies, where the self-assembled film was divided into three zones. Most probably, intermixing and complexation upon adsorption only occur in a region corresponding to the outer zone (III) of their model, although experiments to demonstrate this are still to be performed.

Even for the I(10,NC_3N,PhN_2Pyr)/PVS system, where a lamellar fluctuation extends clearly over the whole film thickness, the word "multilayer" is misleading. The lamellae that appear in the film are generated during the surface-constrained complexation step, starting from prestructured deposits of I(10,NC_3N,PhN_2Pyr). This process occurs over a volume controlled by the range of diffusion of PEL's in the film, which is the blurring step of the process and which prevents true control over layer positioning. Hence, despite the lamellar structure of I(10,NC_3N,PhN_2Pyr)/PVS films, such films should not be considered as true multilayers.

Obviously, the most important step to control in order to construct useful devices is the diffusion step, which is also the less well understood one at the present stage. Possible handles are ionic strength, solvent nature, chemical architecture of the polyions (e.g., rigid platelets), electrostatic forces, etc. Further work is needed to explore these directions. Meanwhile, real layering can only be performed by using systems of the type $((A/B)_m/(C/D)_n)_p$, where $(A/B)_m$ and $(C/D)_n$ should be considered as blend layers defining multilayer structure (provided m and n are sufficiently large).

Finally, note that the decoupling between growth (amounts adsorbed) and structure formation (surface-constrained complexation after PEL diffusion) should allow unprecedented level of control over film architecture and growth. Intelligent molecular design of the PEL chains using concepts from supramolecular chemistry should be used to favor the formation of structured symplexes, without preventing film growth. This however requires a deeper understanding of symplex structuring, which is currently lacking. In addition, as will be shown in a forthcoming paper,[56] the relationship between bulk complex and film structure is far from being simple, given the probable difference in their formation rate and the influence of substrate wall on film structure.

Conclusions

We have presented an in-depth examination of the growth and structure formation of polyelectrolyte self-assemblies (so-called "multilayers") made from a lyotropic ionene and a strong polyelectrolyte. We have shown that highly ordered polyelectrolyte films may be obtained, consisting of a regular lamellar nanostructure extending over considerable distances in the films, with preferential orientation of chain fragments occurring in the films. This is in marked contrast with classical, "fuzzy" multilayers, for which no internal structure was reported so far. From our set of results, including a comparison of the structures of "multilayers" and bulk complexes, we propose that three mechanisms govern film growth and structuring: adsorption of the polyelectrolyte (governed by electrostatic balance), diffusion of the PEL into the previously adsorbed film (which is the blurring step), and surface-constrained complexation between the polyanion and the polycation resulting from the mixing due to diffusion. Depending on whether the polyelectrolytes are capable of forming structured complexes or not, the self-assembled film will present different levels of internal organization. These findings have important implications for the general understanding of electrostatic self-assembly and for possible applications therefrom.

Acknowledgment. The authors thank E. Wischerhoff, P. Fisher, B. Mayer, and M. Koetse for their contribution to the synthesis of the ionene as well as K. Glinel for her contribution to the study of PDADMAC/PSS multilayers. Thanks are due to V. Stone and C. Bollinne for their contribution to XRR development and to B. Nysten for his help with AFM. This research benefited from numerous discussions with P. Bertrand, A. Delcorte, B. Laguitton, and R. Legras. The research was supported by the DG Recherche Scientifique of the French Community of Belgium (Action de Recherches Concertée, convention 94/99-173) and by the Belgian National Fund for Scientific Research.

References and Notes

(1) Fendler, J. H., Ed. *Nanoparticles and Nanostructured Films: Preparation, Characterization and Applications*; Wiley-VCH: Weinheim, 1998.
(2) Ulman, A. *An Introduction to Ultrathin Organic Films: From Langmuir−Blodgett to Self-Assembly*; Academic Press: Boston, 1991.
(3) Petty, M. C. *Langmuir−Blodgett Films: an Introduction*; Cambridge University Press: Cambridge, 1996.
(4) Ulman, A. *Chem. Rev.* **1996**, *96*, 1533.
(5) Decher, G.; Hong, J. D. *Ber. Bunsen-Ges. Phys. Chem.* **1991**, *95*, 1430.
(6) Lvov, Y. M.; Decher, G. *Crystallogr. Rep.* **1994**, *39*, 628.
(7) Sano, M.; Lvov, Y.; Kunitake, T. *Annu. Rev. Mater. Sci.* **1996**, *26*, 153.
(8) Decher, G. In *Comprehensive Supramolecular Chemistry (Templating, Self-Assembly and Self-Organization)*; Sauvage, J.-P., Hosseini, M. W., Eds.; Pergamon Press: Oxford, 1996; Vol. 9, p 507.
(9) Decher, G. In *The Polymer Materials Encyclopedia: Synthesis, Properties, and Applications*; Salamone, J. C., Ed.; CRC Press: Boca Raton, FL, 1996; p 4540.
(10) Knoll, W. *Curr. Opin. Colloid Interface Sci.* **1996**, *1*, 137.
(11) Decher, G. *Science* **1997**, *277*, 1232.
(12) Decher, G.; Eckle, M.; Schmitt, J.; Struth, B. *Curr. Opin. Colloid Interface Sci.* **1998**, *3*, 32.
(13) Raposo, M.; Oliveira, O. N., Jr. *Braz. J. Phys.* **1998**, *28*, 392.
(14) Bertrand, P.; Jonas, A.; Laschewsky, A.; Legras, R. *Macromol. Rapid Commun.* **2000**, *21*, 319.
(15) Arys, X.; Jonas, A. M.; Laschewsky, A.; Legras, R. In *Supramolecular Polymers*; Ciferri, A., Ed.; Marcel Dekker: New York, 2000; p 505.
(16) Ferreira, M.; Cheung, J. H.; Rubner, M. F. *Thin Solid Films* **1994**, *244*, 806.
(17) Hong, J. D.; Lowack, K.; Schmitt, J.; Decher, G. *Prog. Colloid Polym. Sci.* **1993**, *93*, 98.
(18) Lvov, Y.; Decher, G.; Sukhorukov, G. *Macromolecules* **1993**, *26*, 5396.
(19) Cooper, T. M.; Campbell, A. L.; Crane, R. L. *Langmuir* **1995**, *11*, 2713.
(20) Kleinfeld, E. R.; Ferguson, G. S. *Science* **1994**, *265*, 370.
(21) Bliznyuk, V. N.; Tsukruk, V. V. *Polym. Prepr. (Am. Chem. Soc., Div. Polym. Chem.)* **1997**, *38*, 963.
(22) Watanabe, S.; Regen, S. L. *J. Am. Chem. Soc.* **1994**, *116*, 8855.
(23) Hong, H. G. *Bull. Korean Chem. Soc.* **1995**, *16*, 1145.
(24) Lvov, Y.; Haas, H.; Decher, G.; Möhwald, H.; Mikhailov, A.; Mtchedlishvily, B.; Morgunova, E.; Vainshtein, B. *Langmuir* **1994**, *10*, 4232.

(25) Pommersheim, R.; Schrezenmeir, J.; Vogt, W. *Macromol. Chem. Phys.* **1994**, *195*, 1557.
(26) Donath, E.; Sukhorukov, G. B.; Caruso, F.; Davis, S. A.; Möhwald, H. *Angew. Chem., Int. Ed. Engl.* **1998**, *37*, 2202.
(27) Caruso, F.; Caruso, R. A.; Möhwald, H. *Science* **1998**, *282*, 1111.
(28) Möhwald, H. *Colloid Surf. A* **2000**, *171*, 25.
(29) Korneev, D.; Lvov, Y.; Decher, G.; Schmitt, J.; Yaradaikin, S. *Physica B* **1995**, *213/214*, 954.
(30) Kellogg, G. J.; Mayes, A. M.; Stockton, W. B.; Ferreira, M.; Rubner, M. F.; Satija, S. K. *Langmuir* **1996**, *12*, 5109.
(31) Lösche, M.; Schmitt, J.; Decher, G.; Bouwman, W. G.; Kjaer, K. *Macromolecules* **1998**, *31*, 8893.
(32) Decher, G.; Lvov, Y.; Schmitt, J. *Thin Solid Films* **1994**, *244*, 772.
(33) Tarabia, M.; Hong, H.; Davidov, D.; Kirstein, S.; Steitz, R.; Neumann, R.; Avny, Y. *J. Appl. Phys.* **1998**, *83*, 725.
(34) Schmitt, J.; Grünewald, T.; Decher, G.; Pershan, P. S.; Kjaer, K.; Lösche, M. *Macromolecules* **1993**, *26*, 7058.
(35) Hong, H.; Steitz, R.; Kirstein, S.; Davidov, D. *Adv. Mater.* **1998**, *10*, 1104.
(36) Chen, W.; McCarthy, T. J. *Macromolecules* **1997**, *30*, 78.
(37) Liu, Y.; Wang, A.; Claus, R. *J. Phys. Chem. B* **1997**, *101*, 1385.
(38) Hsieh, M. C.; Farris, R. J.; McCarthy, T. J. *Macromolecules* **1997**, *30*, 8453.
(39) Yoo, D.; Shiratori, S. S.; Rubner, M. F. *Macromolecules* **1998**, *31*, 4309.
(40) Joly, S.; Kane, R.; Radzilowski, L.; Wang, T.; Wu, A.; Cohen, R. E.; Thomas, E. L.; Rubner, M. F. *Langmuir* **2000**, *16*, 1354.
(41) Laurent, D.; Schlenoff, J. B. *Langmuir* **1997**, *13*, 1552.
(42) Cassier, T.; Lowack, K.; Decher, G. *Supramol. Sci.* **1998**, *5*, 309.
(43) Baur, J. W.; Rubner, M. F.; Reynolds, J. R.; Kim, S. *Langmuir* **1999**, *15*, 6460.
(44) Kotov, N. A.; Haraszti, T.; Turi, L.; Zavala, G.; Geer, R. E.; Dékány, I.; Fendler, J. H. *J. Am. Chem. Soc.* **1997**, *119*, 6821.
(45) Kim, H. N.; Keller, S. W.; Mallouk, T. E.; Schmitt, J.; Decher, G. *Chem. Mater.* **1997**, *9*, 1414.
(46) Kotov, N. A.; Dékany, I.; Fendler, J. H. *Adv. Mater.* **1996**, *8*, 637.
(47) Lvov, Y.; Essler, F.; Decher, G. *J. Phys. Chem.* **1993**, *97*, 13773.
(48) Kong, W.; Zhang, X.; Gao, M. L.; Zhou, H.; Li, W.; Shen, J. C. *Macromol. Rapid Commun.* **1994**, *15*, 405.
(49) Gao, M.; Kong, X.; Zhang, X.; Shen, J. *Thin Solid Films* **1994**, *244*, 815.
(50) Schmitt, J.; Decher, G.; Dressick, W. J.; Brandow, S. L.; Geer, R. E.; Shashidhar, R.; Calvert, J. M. *Adv. Mater.* **1997**, *9*, 61.
(51) Decher, G., personal communication.
(52) Laschewsky, A.; Mayer, B.; Wischerhoff, E.; Arys, X.; Jonas, A. *Ber. Bunsen-Ges. Phys. Chem.* **1996**, *100*, 1033.
(53) Delcorte, A.; Bertrand, P.; Arys, X.; Jonas, A.; Wischerhoff, E.; Mayer, B.; Laschewsky, A. *Surf. Sci.* **1996**, *366*, 149.
(54) Arys, X.; Jonas, A. M.; Laguitton, B.; Legras, R.; Laschewsky, A.; Wischerhoff, E. *Prog. Org. Coat.* **1998**, *34*, 108.
(55) Fischer, P.; Laschewsky, A.; Wischerhoff, E.; Arys, X.; Jonas, A.; Legras, R. *Macromol. Symp.* **1999**, *137*, 1.
(56) Arys, X.; Wischerhoff, E.; Fischer, P.; Legras, R.; Laschewsky, A.; Jonas, A. M. Second paper of this series, to be submitted.
(57) Glinel, K.; Laschewsky, A.; Jonas, A. M. Third paper of this series, in preparation.
(58) Laschewsky, A.; Wischerhoff, E.; Kauranen, M.; Persoons, A. *Macromolecules* **1997**, *30*, 8034.
(59) Laschewsky, A.; Wischerhoff, E.; Denzinger, S.; Ringsdorf, H.; Delcorte, A.; Bertrand, P. *Chem. Eur. J.* **1997**, *3*, 34.
(60) Elman, J. F.; Johs, B. D.; Long, T. E.; Koberstein, J. T. *Macromolecules* **1994**, *27*, 5341.
(61) Carim, A. H.; Dovek, M. M.; Quate, C. F.; Sinclair, R.; Vorst, C. *Science* **1987**, *237*, 630.
(62) Raposo, M.; Pontes, R. S.; Mattoso, L. H. C.; Oliveira, O. N. *Macromolecules* **1997**, *30*, 6095.
(63) Willstätter, R.; Rohdewald, M. *Hoppe-Seiler's Z. Physiol. Chem.* **1934**, *225*, 103.
(64) Glatter, O.; Kratky, O. *Small-Angle X-ray Scattering*; Academic Press: London, 1982.
(65) Glatter, O. *J. Appl. Crystallogr.* **1974**, *7*, 147.
(66) Stone, V. Interfaces in Multiphasic Polymer-based Materials: a Study on Model Systems of Interdiffusion and Segregation Effects. PhD dissertation, Université catholique de Louvain, Louvain-la-Neuve, Belgium, 1999.
(67) Arys, X. Understanding Ordering in Polyelectrolyte Multilayers: Effect of the Chemical Architecture of the Polycation. PhD dissertation, Université catholique de Louvain, Louvain-la-Neuve, Belgium, 2000.
(68) Kleim, R.; Kuntzler, L.; El Ghemmaz, A. J. *J. Opt. Soc. Am. A* **1994**, *11*, 2550.
(69) Azzam, R. M. A.; Bashara, N. M. *Ellipsometry and Polarized Light*; North-Holland: Amsterdam, 1977.
(70) Aspnes, D. E.; Studna, A. A. *Phys. Rev. B* **1983**, *27*, 985.
(71) Seferis, J. C. In *Polymer Handbook*, 3rd ed.; Brandrup, J., Immergut, E. H., Eds.; John Wiley & Sons: New York, 1989; pp VI/451−VI-461.
(72) Due to the close proximity of the refractive index of the film and of the thin native silicon oxide layer (1.45), it can be shown that ellipsometry essentially determines the sum of the film and native oxide thickness, within 2−3 Å.[67]
(73) Tredgold, R. H. *Order in Thin Organic Films*; Cambridge University Press: New York, 1994.
(74) Bollinne, C.; Stone, V. W.; Carlier, V.; Jonas, A. M. *Macromolecules* **1999**, *32*, 4719.
(75) Pershan, P. S.; Als-Nielsen, J. *Phys. Rev. Lett.* **1984**, *52*, 759.
(76) Singh, N.; Tirrell, M.; Bates, F. S. *J. Appl. Crystallogr.* **1993**, *26*, 650.
(77) Parratt, L. G. *Phys. Rev.* **1954**, *95*, 359.
(78) Parratt, L. G. *J. Chem. Phys.* **1956**, *53*, 597.
(79) Pedersen, J. K.; Hamley, I. W. *J. Appl. Crystallogr.* **1994**, *27*, 36.
(80) Lekner, J. *Theory of Reflection of Electromagnetic and Particle Waves*; Martinus Nijhoff: Dordrecht, 1987.
(81) Zhou, X.-L.; Chen, S. H. *Phys. Rev. E* **1993**, *47*, 3174.
(82) Press, W. H.; Teukolsky, S. A.; Vetterling, W. T.; Flannery, B. P. *Numerical Recipes in C: The Art of Scientific Computing*, 2nd ed.; Cambridge University Press: Cambridge, 1992.
(83) Russell, T. P. *Mater. Sci. Rep.* **1990**, *5*, 171.
(84) We have also performed experiments where samples were dried after each deposition cycle. We did not find significant differences with samples dried only at the end of the fabrication process.
(85) Sukhorukov, G. B.; Donath, E.; Lichtenfeld, H.; Knippel, E.; Knippel, M.; Budde, A.; Möhwald, H. *Colloids Surf. A* **1998**, *137*, 253.
(86) Schlenoff, J. B.; Ly, H.; Li, M. *J. Am. Chem. Soc.* **1998**, *120*, 7626.
(87) Phuvanartnuruks, V.; McCarthy, T. J. *Macromolecules* **1998**, *31*, 1906.
(88) Steitz, R.; Leiner, V.; Siebrecht, R.; Klitzing, R. v. *Colloids Surf. A: Physicochem. Eng. Aspects* **2000**, *163*, 63.
(89) Ladam, G.; Schaad, P.; Voegel, J. C.; Schaaf, P.; Decher, G.; Cuisinier, F. *Langmuir* **2000**, *16*, 1249.
(90) Van Krevelen, D. W. *Properties of Polymers: their Correlation with Chemical Structure; their Numerical Estimation and Prediction from Additive Group Contributions*; Elsevier: Amsterdam, 1990.
(91) Guinier, A. *X-ray Diffraction*; Freeman: San Francisco, 1963.
(92) The good agreement between N_{DS} and film thickness (below 800 Å) validates a posteriori the use of the Debye−Scherrer law to analyze the data. The full width at half-maximum of the Bragg reflection was properly estimated despite the presence of Kiessig fringes which distort the shape of Bragg peaks. This is because the distortion is relatively small when scattered intensity is plotted in a linear scale instead of the logarithmic scale used in Figure 4, even for the thinner films. In addition, we found that N_{DS} agrees well with the number of oscillations found in the density profiles obtained by fitting the reflectivity, for all films for which such a fit was attempted.
(93) Hosemann, R.; Bagchi, S. N. *Direct Analysis of Diffraction by Matter*; North-Holland: Amsterdam, 1962.
(94) The complex made using PSPI also presents a reflection at 27 Å, most probably due to the inclusion of uncomplexed I(10,-NC_3N,ϕN_2Pyr) in the collected powder.
(95) Philipp, B.; Dautzenberg, H.; Linow, K.-J.; Kötz, J.; Dawydoff, W. *Prog. Polym. Sci.* **1989**, *14*, 91.
(96) Smid, J.; Fish, D. In *Encyclopedia of Polymer Science and Engineering*; Mark, H. F., Bikales, N. M., Overberger, C. G., Kroschwitz, J. I., Eds.; John Wiley & Sons: New York, 1988; Vol. 11, pp 720−739.
(97) Farhat, T.; Yassin, G.; Dubas, S. T.; Schlenoff, J. B. *Langmuir* **1999**, *15*, 6621.
(98) Wu, A.; Yoo, D.; Lee, J. K.; Rubner, M. F. *J. Am. Chem. Soc.* **1999**, *121*, 4883.
(99) Rubner, M. *Proc. Am. Chem. Soc. Div. Polym. Mater.: Sci. Eng.* **2000**, *83*, 554.

MA010092S